European Journal of Pharmaceutics and Biopharmaceutics 145 (2019) 42–53

Contents lists available at ScienceDirect

European Journal of Pharmaceutics and Biopharmaceutics

journal homepage: www.elsevier.com/locate/ejpb

Selective anti-ErbB3 aptamer modified sorafenib microparticles: *In vitro* and *in vivo* toxicity assessment

Muhammad Yasir Ali[a,b], Imran Tariq[a,c], Muhammad Farhan Sohail[d], Muhammad Umair Amin[a], Sajid Ali[a], Shashank Reddy Pinnapireddy[a], Asad Ali[e], Jens Schäfer[a], Udo Bakowsky[a,*]

[a] Department of Pharmaceutics and Biopharmaceutics, University of Marburg, Marburg, Germany
[b] Faculty of Pharmaceutical Sciences, GC University Faisalabad, Faisalabad, Pakistan
[c] Punjab University College of Pharmacy, University of the Punjab, Lahore, Pakistan
[d] Riphah Institute of Pharmaceutical Sciences, Riphah International University, Lahore, Pakistan
[e] My Pets Clinic, Bahawalpur, Pakistan

ARTICLE INFO

Keywords:
Polymer
PLGA
CLSM
SEM
Cancer

ABSTRACT

The delivery of aptamer modified therapeutic moieties to specific tissue sites has become one of the major therapeutic choices to reduce the toxicity of inhibitory drugs. Bearing this in mind, the current study was designed using sorafenib (SFB) encapsulated microparticles (MP) prepared with biodegradable poly (D, L-lactic-co-glycolic acid) (PLGA) copolymer. The surfaces of these microparticles were modified with RNA aptamer having a binding affinity towards ErbB3 receptors. SFB-loaded MP (MPS) were prepared by o/w solvent evaporation method and the surface was coupled with the amino group of aptamer by EDC/NHS chemistry. Physiochemical investigations were done by dynamic light scattering, scanning electron microscopy and FTIR. *In vitro* apoptosis assay, cell viability assay and metastatic progression showed a significant decrease ($p < 0.001$) *in vitro* cell viability for MPS and MPS-Apt as compared to MP. The synergistic combination of SFB and aptamer also decreased the metastatic progression of cells for an extended period. Microparticles were also evaluated for *in vivo* toxicity in female BALB/c mice. It was evident that the presence of aptamer decreased the generalized toxicity of MPS-Apt, as measured by mean body weight loss and blood profiles, keeping all the blood formed elements level within acceptable limits. The histopathological investigations showed some necrotic and pyknotic bodies. In a similar fashion, liver function test and renal function tests showed pronounced effects of formulations on vital organs.

1. Introduction

The non-specificity of inhibitory drugs has become one of the major limiting factors in cancer treatment [1,2]. The conventional dosage (either oral or parenteral) forms have also exaggerated this problem either due to their local or systemic effects by the delivery of drug of choice to non-specified sites. Therefore, new therapeutic approaches are heading towards non-conventional dosage forms, such as microparticles and nanoparticles [3]. The inhibitory drugs can be loaded in these particles by entrapment, encapsulation or dissolution [4,5]. Polylactide-co-glycolide (PLGA) has been approved years ago by the FDA due to its biocompatibility and biodegradability as a carrier system. The development of functionalized tumor-specific formulations of PLGA was the prime objective of the current study. These formulations deliver the inhibitory drugs specifically to the tumor, thereby decreasing the overall toxicity towards healthy tissues [1].

Aptamers are chemically synthesized short sequence RNA or DNA and like an antibody, can bind by chemical or electrostatic interactions with specific binding sites. These sites may be specific proteins or receptors in tissues. However, aptamers are superior as compared to the antibodies due to their chemical synthesis, ease of modification, little batch to batch variation, physical stability and less immunogenicity [6,7]. Moreover, they can be attached with carboxylate, sulfhydryl or amino group at one of the prime ends. However, nucleases in eukaryotic cells destabilize them. To overcome this problem, they can be conjugated with small proteins, drug molecules directly or attached on the surface of micro/nanoparticles [8–10].

Amongst the cell membrane receptors, the growth receptors of receptor tyrosine kinase (RTK) family are responsible for cancerous cell growth, proliferation and infiltration into other tissues by migration.

* Corresponding author.
E-mail address: ubakowsky@aol.com (U. Bakowsky).

https://doi.org/10.1016/j.ejpb.2019.10.003
Received 9 August 2019; Received in revised form 11 October 2019; Accepted 14 October 2019
Available online 15 October 2019
0939-6411/

These receptors are also responsible for anti-apoptotic signaling. Epidermal growth factor family (ErbB) is one of the membrane-bound receptors of sub-class of RTK, comprising of four member's viz. ErbB1, ErbB2, ErbB3 and ErbB4. The targeted delivery of inhibitory drugs against these receptors is becoming a leading course in the treatment of cancer [11–13].

Targeted delivery of the microparticles of sorafenib (SFB) using aptamer against ErbB3 was, therefore, the aim of the current study. ErbB3 is responsible for cell progression, proliferation, migration and also inhibition of apoptosis [14]. On the other hand, SFB is a multi-kinase inhibitor, which inhibits VEGFR and platelet-derived growth factor receptor. The administration of SFB inhibited angiogenesis and vasculogenesis [15–17]. Specific inhibition of vessels in tumor micro-environment decreases cancer growth. Therefore, the combination of SFB and aptamer may be used for effectively combating cancer. Moreover, this combination of aptamer and drug may be helpful in specific targeting of the drug towards the overly expressed ErbB3 receptors [17–20].

2. Materials and methods

2.1. Materials

RNA aptamer, (Apt) with 5′ cyanine 5 (Cyn 5) and 3′ C6 amino modifier spacer group

(5′-CAGCGAAAGUUGCGUAUGGGUCACAUCGCAG-3′) was purchased from Eurogentec (Seraing, Belgium). PLGA (R503H, Mw30 kDa) was obtained from Evonic (Darmstadt, Germany). 1-ethyl-3-(3-dimethylaminopropyl)-carbodiimide (EDC), N-hydroxysuccinimide (NHS), 3-(4,5-dimethyl-2-thiazolyl)-2,5-diphenyl-2H-tetrazolium bromide (MTT), 2′,7′-dichlorofluorescein diacetate (DCFDA) and *tert*-butyl hydroperoxide (TBHP) were purchased from Sigma Aldrich (Darmstadt, Germany). 2-(*N*-morpholino) ethane sulfonic acid (MES) was purchased from Serva (Heidelberg, Germany). Poly-vinyl-alcohol (Mowiol 4–88) was a gift sample from Kuraray (Hattersheim, Germany). Sorafenib was purchased from LC Laboratories (Woburn, USA). Ethyl acetate, tetrahydrofuran and ethanol were obtained from Chemsolute-Th. Geyer (Renningen, Germany), Carl Roth (Karlsruhe, Germany) and Fisher Scientific (Schwerte, Germany) respectively. All the reagents used were of analytical grade.

2.2. Cell lines and cell culture

Breast cancer cell line MDA-MB-231 expressing ErbB3 was purchased from ATCC Manassas, USA. Cells were cultured in DMEM (Capricorn Scientific, Ebsdorfergrund, Germany) medium supplemented with 10 % fetal bovine serum (Sigma Aldrich). Cells were maintained at 37 °C and 7 % CO_2 under humid conditions.

2.3. Preparation of microparticles

PLGA (R503 H) microparticles (MP) were prepared by oil in water emulsion solvent evaporation method. Briefly, a weighed amount of PLGA was dissolved in 10 ml of ethyl acetate. 0.25 % PVA solution was prepared in ultra-pure water (Purelab Flex 4, Elga Labwater, High Wycombe, UK) and filtered using a 200 nm syringe filter. The organic phase was added drop-wise to 10 ml of the aqueous phase. 30 ml of ultra-pure water was added to facilitate organic solvent evaporation under constant stirring for 24 h. Drug-loaded microparticles (MPS) were prepared by the same method, except that sorafenib was dissolved in THF:EtOH (4:1) and mixed with PLGA solution in ethyl acetate, the rest of the method was same as above.

2.4. Encapsulation efficiency and in vitro release profile

MPS were centrifuged (Eppendorf centrifuge 5418, Eppendorf, Germany) at 12,000 rcf for 15 min. The supernatant was removed and the pellet was dissolved in DMSO. Samples were analyzed by UV spectrophotometry (UV mini 1240, Shimadzu, Japan) at 265 nm. A calibration curve was recorded with known concentrations of SFB. The solvent background was recorded from microparticles without drug and encapsulation efficiency was calculated using the following equation:

$$EE(\%) = \frac{Amount\ \ of\ \ drug\ \ in\ \ MPS}{Amount\ \ of\ \ drug\ \ loaded} * 100$$

The release profile of SFB from PLGA microparticles was evaluated in PBS (pH 7.4) with 1% v/v Tween 80.1 ml of microparticle suspension was washed thrice with PBS, followed by centrifugation at 12,000 rcf for 10 min. Pellet was resuspended in 1 ml PBS with 1% Tween 80 and placed into an orbital shaker (KS4000 IC, IKA Werke, Staufen, Germany) at 150 rpm and 37 ± 0.5 °C. The samples were removed at designated time intervals. After centrifugation, the pellets were re-suspended in 1 ml PBS (pH 7.4)/1% Tween 80 and returned back to the shaker. At defined time intervals, pellets were dissolved in 1 ml DMSO and absorbance was measured at 265 nm. The vehicle background was then subtracted by measuring the pellet of PLGA microparticles without SFB, prepared under the same conditions.

2.5. Surface modification of microparticles

Surface coupling reaction (EDC/NHS) was employed for modification of the surfaces of the microparticles. Microparticles were washed with ultra-pure water by centrifugation and resuspended in MES buffer (pH 5.5). They were then treated with 400 mM EDC and 200 mM NHS for 30 min. NHS group barring microparticles were treated with a primary amine of aptamer (Apt) at a microparticle:aptamer ratio of 1:12. After 2 h reaction time, washing was done using ultra-pure water and microparticles were resuspended in purified water. These modified microparticles were stored at 4 °C until further use.

2.6. Aptamer coupling

The presence of Apt on the surfaces of microparticles was quantified by fluorescence assessment of Cyn 5. Freshly prepared surface-modified microparticles were washed three times with ultra-pure water followed by centrifugation at 12,000 rcf for 10 min. Fluorescence of the supernatant and the pellet was quantified using FLUOStar Optima plate reader (BMG Labtech, Offenburg, Germany) at $\lambda_{ex}/\lambda_{em}$630 nm/670 nm and calculated by using the above-mentioned equation.

2.7. FTIR spectroscopy

The coupling of Apt on the surfaces of microparticles was also assessed by Fourier transform infrared spectroscope equipped with a single reflection diamond ATR module (Alpha-P, Bruker, Massachusetts, USA). Freeze-dried microparticles were loaded onto ATR platinum diamond crystal. Background correction was done in the absence of any sample. The average of 18 scans at a spectral resolution of 2 cm^{-1} was taken automatically to obtain each spectrum. The spectrum was collected in a range between 4000 cm^{-1} and 400 cm^{-1} and was represented as percentage transmittance.

2.8. Physicochemical characterization

For all prepared formulations, the size distribution was measured by dynamic light scattering (DLS) using Zetasizer Nano ZS (Malvern Instruments, Malvern, UK). Samples were diluted 1:50 with ultra-pure water. Before the measurement, the sample temperature was equilibrated to 25 °C. All measurements were done in triplicates and the sub runs were adjusted by the instrument automatically. Zeta potential was assessed by laser doppler velocimetry (LDV) using the same instrument at a conductivity < 100 µS/cm.

2.9. Scanning electron microscopy (SEM)

Hitachi S-510 scanning electron microscope (Hitachi-High Technologies Europe GmbH, Krefeld, Germany) was used for the morphological analysis. Briefly, 20 µl samples were applied onto specimen stubs with conductive carbon tabs (PLANO Leit-Tabs; Ø 9 mm) and left to dry under a laminar airflow hood. The samples were then sputter-coated with gold at 13.3 Pa Argon using an Edwards S150 sputter coater (Edwards Vacuum, Crawley, UK) and were examined under an accelerating voltage of 5 kV and a working distance of 12 mm under 5.3×10^{-4} Pa vacuum [21]. The signals were processed digitally by DISS 5 digital image acquisition system (Point Electronic GmbH, Halle, Germany).

2.10. In vitro cell viability

In vitro anticancer efficacy of formulations was assessed by MTT assay. Briefly, 10,000 MDA-MB-231 cells/well (0.35 cm^2) were seeded in a 96-well plate and were incubated for 24 h. Series of PLGA microparticles were made in the media and 100 µl/well was added to 96 well plates [21]. The untreated cells were considered as a negative control whereas SFB treated cells were considered as a positive control. After 5 h of incubation, the medium was removed and replaced with fresh medium and incubated further. Plates were allowed to incubate overnight. Next day, the medium was removed and replaced with 2 mg/ml MTT reagent containing medium and incubated for 4 h. The resultant formazan crystals were dissolved using DMSO and absorbance was measured in a FluoStar Optima plate reader at 570 nm. The experiment was repeated three times and the percentage cell viability was calculated. IC_{50} values were calculated by the concentration of microparticles with 50% of the cell survival.

2.11. Apoptosis assay

MDA-MB-231 cells were cultured on sterile coverslips in 24 well plates at a seeding density of 50,000 cells per well (1.8 cm^2) for 24 h. Cells were washed thrice with cold PBS buffer (pH 7.4). 500 µl of different formulations were added to the wells. After 12 h, cells were washed again with PBS and fixed using 4 % paraformaldehyde for 15 min. Cells were counterstained using DAPI (0.1 mg/ml) solution for 20 min. Washing was performed with PBS and cells were examined using a fluorescence microscope (CKX53, Olympus, Tokyo, Japan).

2.12. Cell migration

Inhibition of cell migration and metastasis was evaluated by wound healing assay. MDA-MB-231cells were seeded in 24 well plates. After 24 h, cells were treated with formulations containing 5 µM SFB for 2 h in serum-free medium. A scratch was made with a 200 µl pipette tip. Cells were then washed twice with ice-cold PBS (pH 7.4) and fresh medium was added. Wound closure was observed using an inverted microscope at 0 h, 4 h and 24 h. The raw data was analyzed by SketchAndCalc™ and Gimp 2.10.6® application software. Cell migration and percentage wound healing were calculated measuring the distance between wound closures.

2.13. Reactive oxygen species assessment

Determination of ROS production was done using 2′,7′-dichlorodihydrofluorescein diacetate (carboxy-H_2DCFDA) conversion into 2′,7′-dichlorofluorescein (DCF) as previously reported [22]. Briefly, MDA-MB-231 cells grown in 96 well plates for 24 h were washed (PBS buffer; pH 7.4) and incubated with phenol red-free medium containing 25 µM of carboxy-H_2DCFDA for 30 min. The cells were subsequently washed twice with PBS. Cells were then treated with formulations containing 1.0 µM and 1.5 µM of SFB. After 45 min, cells were washed again with PBS and lysed using lysis reagent (Promega, Mannheim, Germany). The fluorescence was observed at λ_{ex} 485 nm/ λ_{em} 520 nm using a FluoStar Optima plate reader.

2.14. Cellular uptake

For cellular uptake studies, MDA-MB-231 cells were cultured on sterile coverslips in 12-well plates at a seeding density of 90,000 cells per well (3.5 cm^2). After 24 h, the supernatant was removed and washed three times with PBS (pH 7.4). Cells were incubated for 2 h with different formulations. After washing with PBS cells were fixed with 4% paraformaldehyde for 15 min. Cell nucleus was then counterstained with DAPI (0.1 µg/ml) for 10 min in the dark. Cells were washed three times with PBS and the coverslips were mounted on to glass slides and with FluorSave (Calbiochem Corp, La Jolla, USA). Uptake analysis was performed using a confocal laser-scanning microscope (LSM700, Carl Zeiss, Jena, Germany).

2.15. Acute toxicity assessment

Female BALB/c (8–10 weeks old) mice weighing 31.1 ± 2.6 g, were divided into 6 groups (n = 3) and with free access of food and water (*ad libitum*). Experimental protocols were approved by the GC University animal experiment and ethical committee and were performed in collaboration with the in-house facility of My Pets clinic for clinical investigations. The animals were kept at 40% humidity and a temperature of 22 ± 2 °C. The dose of the microparticles was equivalent to the 10 mg/kg dose of SFB. The first group was treated with MP, second with MP-Apt, third with MPS and fourth with MPS-Apt. One group was administered with the aptamer. Normal saline-treated group was considered as control. The particle suspension was injected in the peritoneal cavity using a 26G syringe needle in two equally divided doses on day 1and day 3. The mice were kept under observation for 7 days for alteration in body weight and visual observations for mortality, skin, sleek of fur, urine color, feces, salivation, respiration, eyes and sleep pattern and day-by-day signs of illness. On day 7, complete blood analysis was done and mice were euthanized for tissue histology studies. The vital organs (heart, liver, kidneys and lungs) were removed, carefully washed with normal saline and weighed. The comparison was made with weights of control, and the visceral index was calculated by the following equation:

$$\text{Visceral Index} = \frac{\text{Organ Weight}}{\text{Body Weight}} \times 100$$

2.15.1. Blood biochemistry

Blood was drawn by intra-cardiac injection before euthanizing the mice. The effect of administration of microparticles on the biochemical markers of the blood was observed on the 7th day. These markers include complete blood count (CBC), liver function test (LFT), renal function test (RFT) and total plasma protein.

2.15.2. RBC aggregation test

To determine the compatibility of the formulations with blood, mice erythrocytes were incubated with different formulations. Briefly, red blood cells (RBC) were obtained by centrifugation of fresh blood in tubes containing EDTA. The RBC pellet was washed thrice with PBS (pH 7.4) and diluted to 1:10 with the same. The RBC were incubated with the formulations for 30 min at 37 °C. Centrifugation was done at 500 rcf and the pellet was washed with PBS [23]. The cell suspension was directly observed under a light microscope.

2.15.3. Histopathology

Heart, liver, kidney and lungs were removed after euthanizing the mice and washed with PBS (pH 7.4). These organs were visually

inspected for lesions and any abnormality. The organs were placed in 4% formalin solution for 24 h. Dehydration with gradient ethanol and fixation in paraffin wax blocks was done. Sections of 1 μm were cut carefully with a rotary microtome (Hunan Kaida Scientific Instruments, China) and were transferred to a glass slide. Staining was done with H & E stains and tissues were observed under a microscope (Olympus BX51M, Tokyo, Japan) for any sign of toxicity [24].

2.16. Statistical analysis

GraphPad Prism, v.8.0.1 was used for statistical analysis and comparison. All the values were presented as mean ± standard deviation unless otherwise stated after repeating all the experiments three times. One way ANOVA was performed to identify statistically significant differences with probability values of < 0.05. Statistical differences were denoted as "*" $p < 0.05$, "**" $p < 0.01$ and "***" $p < 0.001$.

3. Results and discussion

3.1. Encapsulation efficiency and in vitro release profile

The encapsulation efficiency of SFB in microparticles was 74.0 ± 5%. Once incorporated, the amount of SFB, released from MPS, was calculated in percentage. It is clear from Fig. 1A that nearly 70% of SFB was released from MPS within the first 24 h. This represented the initial burst release of drug from the surfaces of microparticles. Approximately, 10% SFB was released in the remaining time of release study. This second phase of release represented the combination of diffusion and erosion process of PLGA polymeric chains in microparticles as reported previously [25–27].

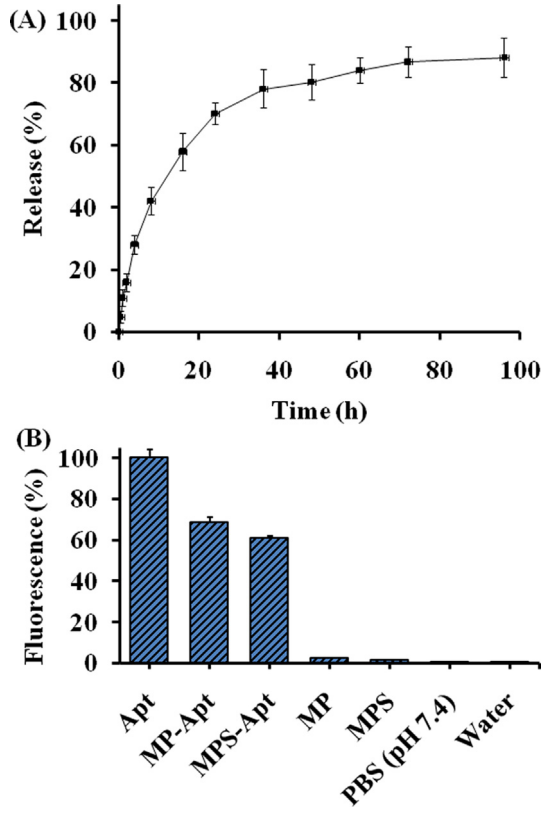

Fig. 1. (A) Release profile of Sorafenib from PLGA microparticles. (B) Fluorescence analysis of Apt at $\lambda_{ex}/\lambda_{em}$ 610/650 nm on blank microparticles (MP) and sorafenib-loaded microparticles (MPS), the fluorescence of Cyn 5 of pure Apt was considered as a reference.

3.2. Aptamer coupling

Binding of Apt on the surface of microparticles was evaluated by fluorescence analysis. The fluorescence analysis at λ_{ex} 610 nm and λ_{em} 650 nm confirmed the attachment of Cyn 5 tagged Apt on the surfaces of microparticles. The results showed that 68.36 ± 2.69 and 60.75 ± 1.02% of Apt was present on the surface of MP and MPS respectively (Fig. 1B).

3.3. FTIR spectroscopy

Identification of different functional groups was done by ATR-FTIR. Hence, the presence of SFB and Apt was also confirmed from the FTIR spectrum. MP showed a characteristic peak of the carboxylic acid of PLGA at 1750 cm^{-1}. The stretching peak of alkene of SFB was present at 1501 cm^{-1}in MPS. Moreover, conjugated carboxylic acid stretching peaks seen at 1700 cm^{-1} along with imine peaks at 1648 cm^{-1} confirmed the attachment of Apt on the surfaces of MP-Apt and MPS-Apt (see supplementary data, S1). The results show the presence of Apt as well as SFB in different formulations. This confirms the formation of microparticles along with successful surface modification.

3.4. Physicochemical characterization

SFB is a poorly water-soluble drug which is readily soluble in DMSO. Its solubility may be increased by co-solvency. Therefore, THF:EtOH (4:1) was used to solubilize SFB and an o/w emulsion was prepared for microparticle preparation. The particle diameter (hydrodynamic diameter as a function of intensity) measured by DLS showed an increase with the addition of drug and aptamer (Fig. 2A). On the other hand, the zeta potential measured was negative in all cases with a maximum of −25.3 ± 2.2 for MP-Apt. Hydrodynamic diameter and zeta potential are influenced by pH and ionic concentrations. Therefore, the presence of SFB changed the diameter and zeta potential of formulations. On the other hand, the amide bond formed between the carboxylic group of PLGA and the amine of aptamer resulted in the attachment of aptamer onto the surface of particles (as shown by FTIR results). This is evident from the change in diameter and zeta potential.

Morphological characterization was done by scanning electron microscopy. Samples were dried under laminar airflow hood on conductive carbon tabs. This resulted in the settlement of microparticles while at the same time maintaining their structure. SEM analysis revealed a smooth surface with a diverse range of sizes was seen in the micrographs (Fig. 2B, 2C). The sizes were between 0.5 and 0.7 μm, which were smaller than those measured by DLS. This was due to the presence of an electrical double layer on the surface of microparticles when measured in suspension form by DLS, whereas for SEM, the particles are measured in vacuum.

3.5. In vitro cell viability

The assessment of cell viability in the presence of formulations was done by MTT assay. The presence of both SFB and Apt resulted in a decrease in cell viability, with maximum effect at highest concentrations (3 μM SFB or equivalent). This response was dose-dependent i.e. increasing with decreasing the dose of the microparticles and vice versa. Therefore, the lowest dose of the formulations (0.19 μM SFB or equivalent) showed a viability of 84.6 ± 2.3% for MPS-Apt and to 92.2 ± 1.5% in the case of MP-Apt. The inhibitory response was strongest in all cases when compared with MP at highest concentration with $p < 0.001$ and showed $p < 0.01$ at the lowest concentration. The IC_{50} value was 1 μM for MPS-Apt. Moreover, MP showed more than 80% cell viability even at the highest concentration (Fig. 3A). This suggested that formulations are relatively safe in the absence of SFB or Apt. Pure SFB (in THF:EtOH) and MPS-Apt itself showed nearly 20% and 42% cell viabilities respectively at highest concentrations. On the

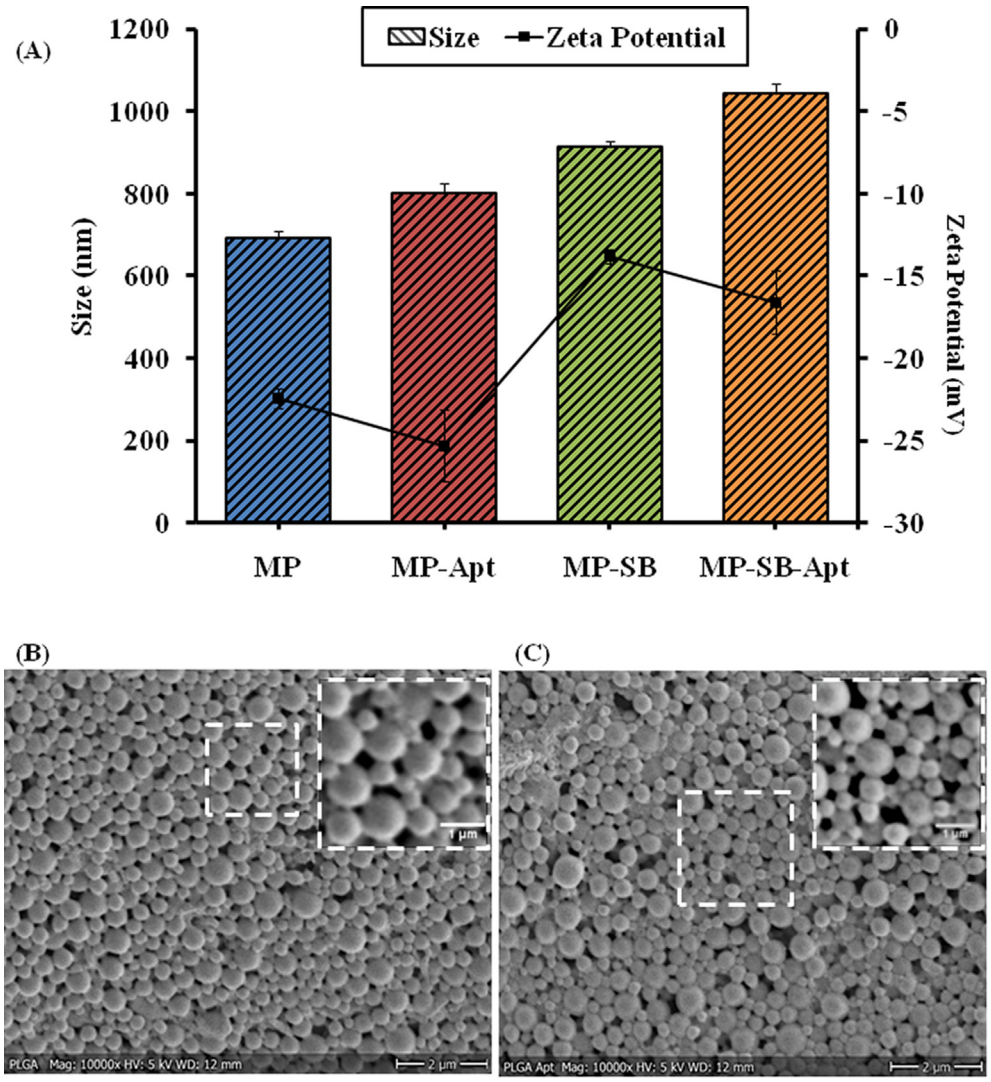

Fig. 2. Physicochemical characterization of microparticles: (A) size and zeta potential of microparticles (MP), surface-modified microparticles (MP-Apt), sorafenib-loaded microparticles (MPS) and sorafenib-loaded surface-modified microparticle (MPS-Apt); (B) SEM micrographs, of MP and (C) MP-Apt. Scale bar represents 2 µm for the micrograph and 1 µm for the inset.

other hand, the solvent THF:EtOH alone showed nearly 66% cell viability (data not shown). Conclusively, the presence of SFB in MPS-Apt showed nearly similar cell viability to that of SFB. The presence of aptamer in the formulations showed an increase in the inhibitory effect due to the presence of the drug on one hand and due to targeted delivery of the formulations in the presence of aptamer [28–30]. The combination of SFB and Apt exhibited targeted SFB microsphere delivery towards ErbB3 rich cells thereby addressing the problem of generalized toxicity due to non-specific drug delivery.

3.6. Apoptosis assay

DAPI was used to analyze the cell death mechanism. DAPI is a nuclear stain, which binds to double-stranded DNA and can detect the chromatin or nuclear condensation and helps localize the formation of apoptotic bodies, which result ultimately in the death of cells. Cell shrinkage, loss of cell membrane, blebbing and chromatin along with nuclear condensations can be observed using this assay [31,32]. The untreated cells did not show any sign of apoptotic body formation. On the other hand, MP showed some cells with nuclear condensation. The cells treated with microparticles in the presence of SFB and/Apt showed nuclear condensation and chromatin degradation [33]. Nuclear blebbing was also prominent due to the presence of SFB and Apt (Fig. 3B). Therefore, the formation of apoptotic bodies was potentiated in the presence of both SFB and Apt, revealing the synergism amongst them.

3.7. Cell migration

Cell migration assay was performed to investigate the effectiveness of SFB and Apt in inhibition of cell proliferation. This was directly observed by an inverted microscope and percentage migration was calculated. It was obvious from the results that the presence of either SFB or aptamer caused the inhibition of migration. The inhibition was strongest at 24 h ($p < 0.001$) for MPS-Apt when compared with control (untreated cells). In the absence of aptamer, after 24 h, cells treated with MPS showed more migration (Fig. 4). These results depicted the synergistic effect of SFB and aptamer together. Both SFB and aptamer complemented the effects of each other. The absence of SFB and Apt resulted in complete healing of wound within 24 h of scratching. The blank formulation (MP) also caused inhibition of wound healing up to 24 h. This was in accordance with cell proliferation assay showing decreased cell viability in the presence of MP (80%).

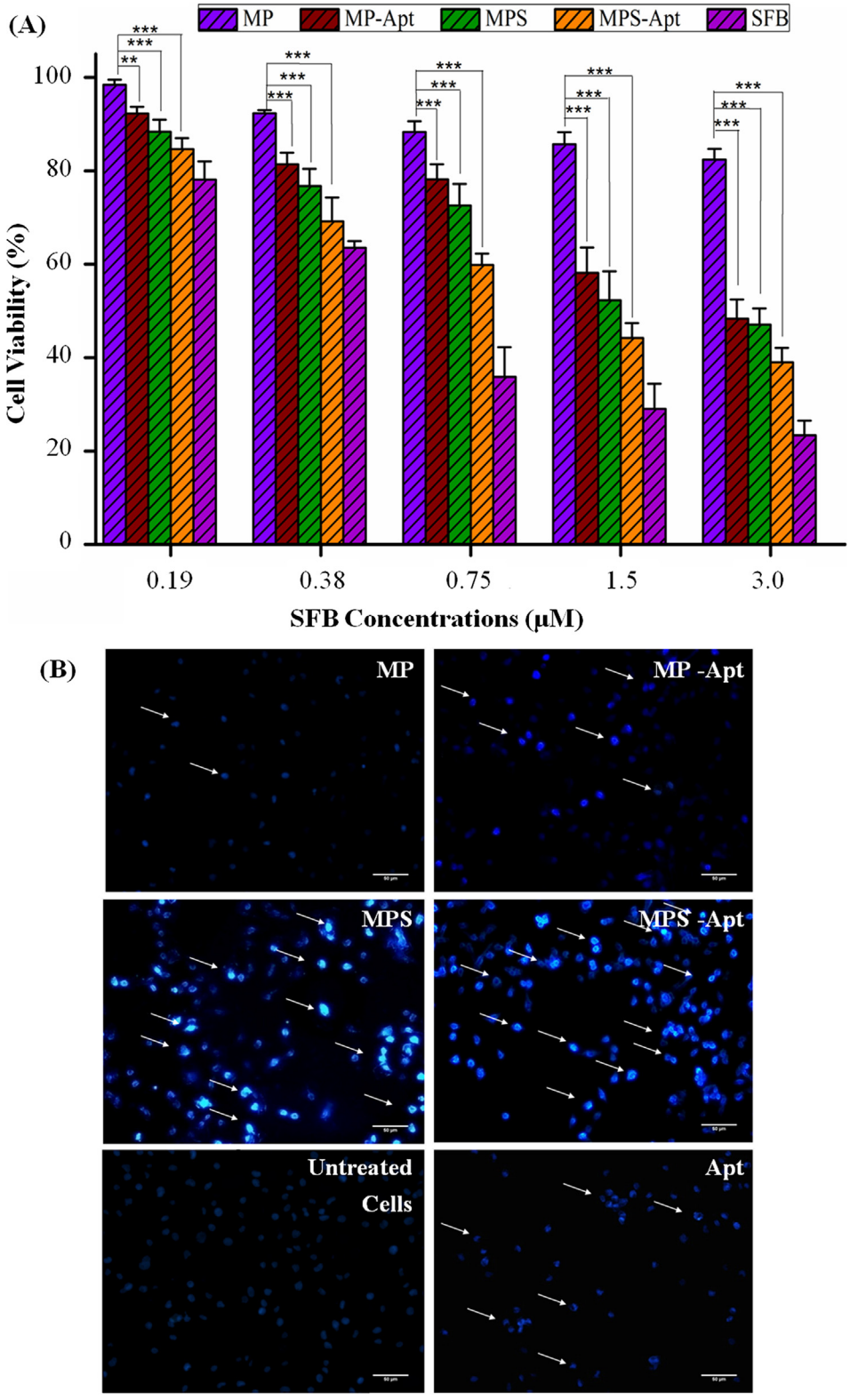

Fig. 3. (A) *In vitro* cell viability. (B) Apoptosis assay showing nuclear condensation and chromatin fragmentation of microparticles (MP), surface-modified microparticles (MP-Apt), sorafenib-loaded microparticles (MPS) and sorafenib-loaded surface-modified microparticle (MPS-Apt). Statistical differences are denoted as "**" $p < 0.01$ and "***" $p < 0.001$.

3.8. Reactive oxygen species assessment

Reactive oxygen species (ROS) can convert carboxy-H_2DCFDA into DCF. The results showed dose-dependent ROS production in the presence of both drug only and drug-aptamer formulations (Fig. 5). In the presence of both the SFB and aptamer, ROS was significantly high compared to the blank formulation (MP). The release of the SFB inside cells caused the production of ROS due to the production NADPH oxidase in mitochondria. This is the proposed mechanism of ROS production in the presence of SFB [34]. However, in the presence of a

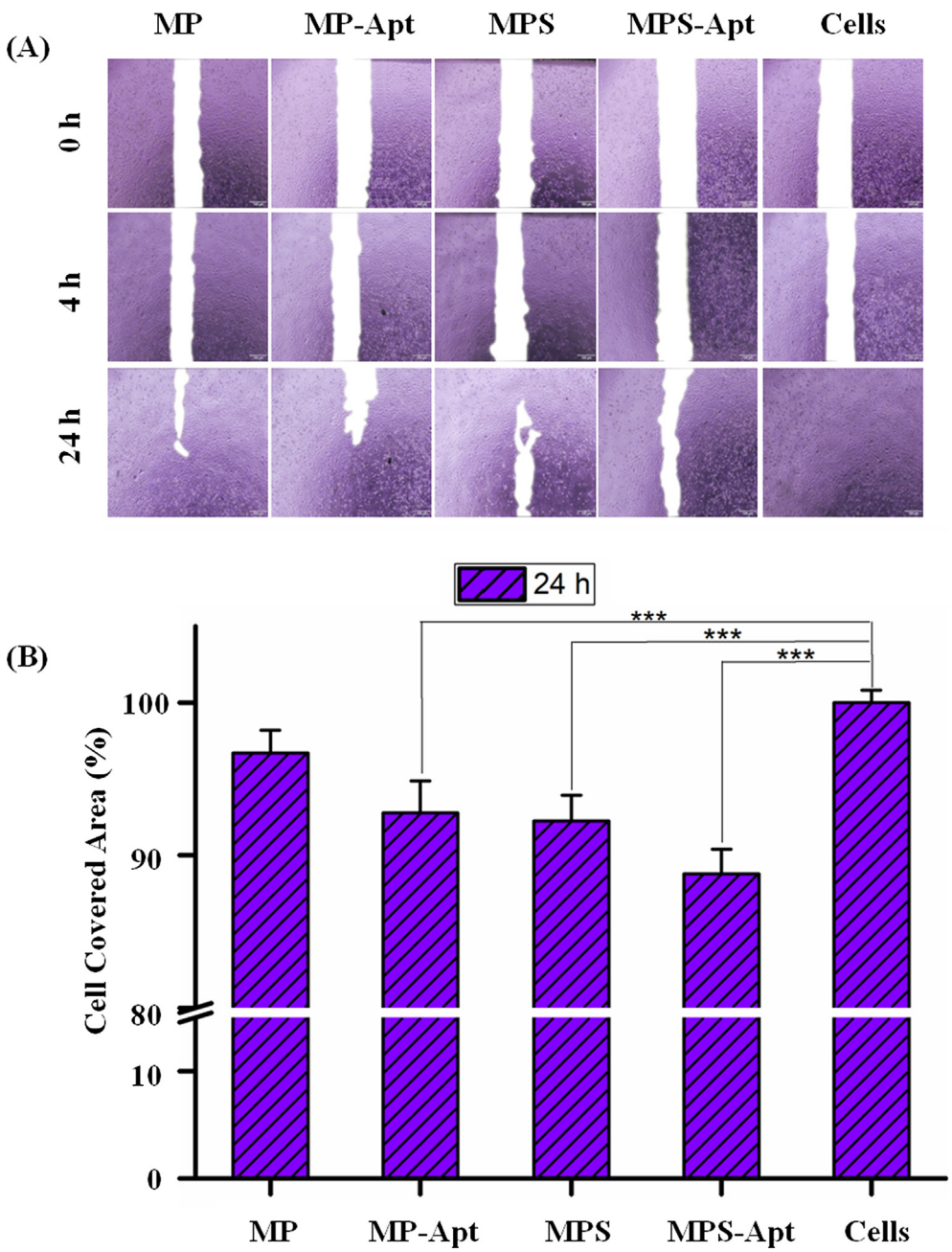

Fig. 4. Effect of formulations on cell migration; scratch was applied using 200 µl pipette tip: (A) wound healing by scratch test; (B) Time-dependent wound healing of microparticles (MP), surface-modified microparticles (MP-Apt), sorafenib-loaded microparticles (MPS) and sorafenib-loaded surface-modified microparticle (MPS-Apt). Statistical differences are denoted as "**" $p < 0.01$ and "***" $p < 0.001$.

higher concentration of SFB, low amounts of ROS were produced. This was the result of the cell death caused by the higher concentrations of SFB. The presence of anti-ErbB3 Apt caused increased production of ROS in combination with SFB [35].

3.9. Cellular uptake

Cellular uptake was visualized by confocal laser scanning microscopy (CLSM). Cyn 5 was attached to 5′ end of the aptamer, which was bound to surface of microparticles. The nucleus of the cell incubated with the formulations was stained with DAPI. CLSM images showed the presence of surface-modified microparticles within the cells. The red fluorescence of aptamer can be seen throughout the cytoplasm, particularly near the nucleus.

ErbB3 receptor-mediated internalization might be the possible mechanism for the toxicity of SFB. These endosomes containing the microparticles released their contents inside the nucleus. This nuclear trafficking of ErbB3 by the endocytosis has been previously reported [36,37]. The z-stack images showed the presence of Cyn 5 labeled aptamer within the nuclear region (Fig. 6A). The intensity plot for co-localization shows DAPI on the x-axis and Cyn 5 on the y-axis. Co-localization coefficient was measured by ZEN software (Carl Zeiss, Jena, Germany). This ranges from 0 to 1, where 0 shows no co-localization and 1 shows 100% co-localization. Co-localization coefficients were above 0.7 in all cases. This explains nearly co-localized particles in the nuclear region. The intensity plot depicted the more intense fluorescence of Cyn 5 channel in case of aptamer treated cells whereas the opposite was true for MPS-Apt treated cells. However, in the MP-Apt treated cells, these channels were almost equally co-localized (Fig. 6B). Aptamer delivered the microparticles to the nucleus, therefore DAPI

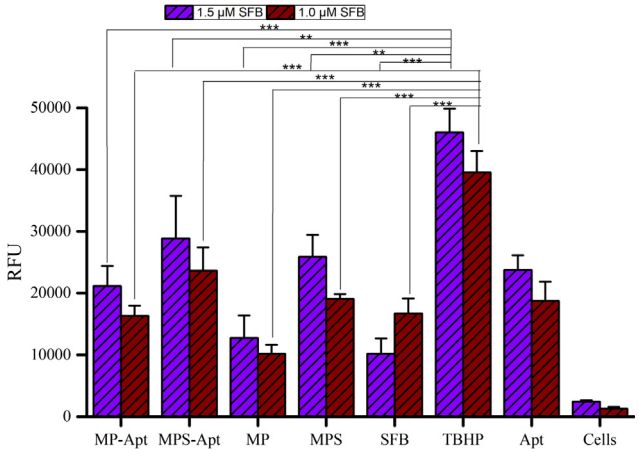

Fig. 5. ROS assay measuring the production of 2′, 7′-dichlorofluorescein (DCF) of microparticles (MP), surface-modified microparticles (MP-Apt), sorafenib-loaded microparticles (MPS) and sorafenib-loaded surface-modified microparticle (MPS-Apt). Tert-butyl hydroperoxide (TBHP) was used as a positive control. Cells indicate untreated cells. Statistical differences are denoted as "**" $p < 0.01$ and "***" $p < 0.001$.

and Cyn 5 fluorescence was nearly equally co-localized in case of MP-Apt. The aptamer, therefore, resulted in enhanced delivery of SFB to the cells rich in ErbB3 receptors.

3.10. In vivo acute toxicity

Female BALB/c mice were injected (intra-peritoneal) with different formulations of microparticles; aptamer and normal saline were used as controls. Mice were observed for 7 days after injection for any abnormal behavior, skin, sleek of fur, urine color, feces, salivation, respiration, eyes and sleep patterns. All the mice survived and showed no physical or behavioral changes. A record of body weight was performed to calculate percentage change on day 7. All these parameters remained unchanged in all cases, except for MPS treated group. The body weight on day 7in MPS treated group decreased by 3.30%. In all other groups, there was an increase in the body weight from nearly 3 to 8% confirming the safety of the formulations (Table 1A). The second assessment was the effect of formulations on body viscera. The presence of SFB and Apt produced a pronounced effect on the visceral index (Table 1B). There was little increase in visceral indices of heart and liver in case of the aptamer, MP-Apt and MPS-Apt groups.

The effect of microparticles on the blood profiles of the mice was also investigated (Table 1C). There were major differences in the values of total leukocyte count ($p < 0.001$). Hemoglobin concentrations also changed, but only slightly with significantly lower levels in case of MPS-Apt ($p < 0.001$) and MPS ($p < 0.001$). However, in the case of the aptamer change was less significant ($p < 0.05$) indicating a less pronounced effect on hemoglobin. These results showed that the formulations altered the normal physiological values of mice used in the study. As reported previously, the presence of anti-ErbB3 agents (aptamer in our case)altered the immune response and was responsible for decreased TLC levels, causing a decrease in the inflammatory response [38,39]. This surface-functionalized therapy can be safe for i.v administration because all the changes were within acceptable limits.

3.10.1. Blood biochemistry

The effects of different formulation on the blood clinical markers i.e. liver function test and kidney function test were investigated (Fig. 7). Nearly in all the treatment groups, alanine aminotransferase (ALT) and aspartate aminotransferase (AST) increased significantly ($p < 0.001$). Exceptions were in the case of MP (ALT) and MP-Apt (AST), where no profound change was observed. These elevated levels after treatment were representative of cardiac problems and non-alcoholic fatty liver. Moreover, AST to ALT ratio was more than 3, which was indicative of liver inflammation, fatty liver and cardiac injury. These results were in accordance with the results of body visceral indices. A decrease in total serum proteins and a slight increase in bilirubin also predicted liver malfunctioning, usually associated with fatty liver [40,41]. Kidney function tests (Fig. 7B) included uric acid, creatinine and blood urea nitrogen (BUN). The values changed significantly ($p < 0.01$ or $p < 0.001$) in all cases, except MP-Apt in the case of uric acid. The concentrations of these markers indicated the poor kidney function or malfunctioning of the liver [41]. Liver and heart muscles are usually rich in ErbB3 receptors. Therefore, the attachment of aptamer on the surface of microparticles mediated their delivery to the organs rich in ErbB3 receptors, resulting in a change in the normal physiology of these organs.

3.10.2. RBC aggregation test

Red blood cell (RBC) aggregation test was performed to monitor the effect of formulations on erythrocytes. The presence of SFB and Apt showed minor structural and morphological changes in RBCs (see Fig. 8A and S2). These results were in accordance with the ROS assay. ROS induced RBCs damage is one of the well-known mechanisms. A synergistic effect was observed in the presence of both SFB and Apt. However, the damage was not too much to damage the RBC morphology completely. The results of the RBC aggregation test were comparable to those of the CBC profile (Table 1C). CBC profile showed a small decrease in RBC count in case of formulations containing SFB and Apt. Their presence caused an increase in RBC aggregation and destruction; hence hematocrit increased. However, these were within the normal range [42,43].

3.10.3. Histopathology

The histopathological investigation was done for heart, liver, kidney and lung (see Fig. 8B and S2). It was obvious from the results that mild to moderate toxicity was seen in the case of heart muscles. Necrosis, infiltration of leukocyte, mild granulative tissue and collagen accumulation were observed in the case of aptamer and formulations containing either both SFB and Apt or alone. These results were in accordance with the body visceral index and plasma profile as heart weight increased in these cases as compared to the control group. Liver showed signs of fibrosis, pyknosis (condensation of nuclei due to apoptosis) and micro and macrovesicular fatty changes. The anisokaryosis (larger nuclei) and binucleated hepatocytes suggested regenerative responses as well as the fatty degeneration mostly in case of MP-Apt and MPS-Apt [44]. Some brown necrotic bodies were also visible. Kidneys did not show any major changes in any of the treatment groups. These findings demonstrated the presence of mild nephritis. On the other hand, no major change in lung histology was also obvious. Normal alveolar structures were observed and arterioles were normal. These investigations reported the safety of this surface-functionalized system.

4. Conclusion

The aim of this study was to formulate functionalized PLGA-SFB microparticles for targeted therapy. The microparticles were modified with the aptamer against ErbB3 receptors, aiming to diminish the toxicity of SFB due to non-specific delivery. Physicochemical and morphological studies revealed a sub-micron range formulation with a spherical and smooth surface. Synergistic dose-dependent cytotoxicity was demonstrated using SFB and Apt formulations. This effect was also evident in apoptosis assay showing nuclear condensation as a possible mechanism of cell death. Inhibition of cell migration by SFB and Apt containing formulations was also revealed from the scratch test. Increased levels of ROS were observed in cells treated with formulations containing both SFB and Apt. The presence of particles, inside

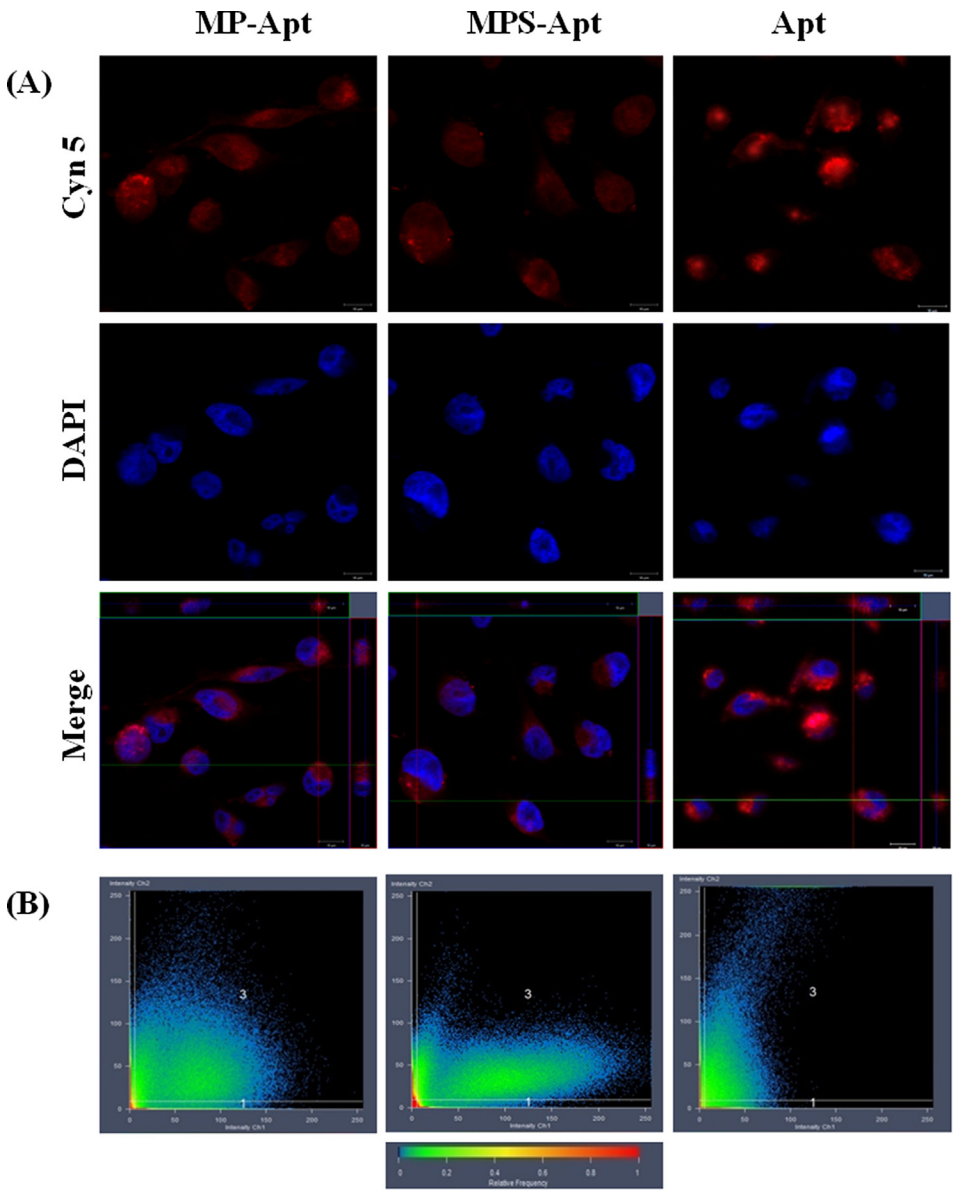

Fig. 6. Cellular uptake in MDA-MB-231 cells: (A) Cellular uptake of Cyn 5 labeled microparticles; images are represented as individual channels and a merged image in the form of z-stack to visualize the presence of aptamer functionalized microparticles near nucleus; (B) Co-localization of surface-modified microparticles (MP-Apt), sorafenib-loaded surface-modified microparticle (MPS-Apt) and aptamer (Apt) treated cells.

Table 1A
Bodyweight changes in mice in different treatment groups.

Treatments	Body Wt. Start (gm ± SD)	Body Wt. End (gm ± SD)	Change (%)
MP	34.13 ± 1.54	35.07 ± 1.77	2.66
MP-Apt	30.43 ± 1.18	32.43 ± 2.59	6.17
MPS	32.30 ± 4.90	31.27 ± 4.82	−3.30
MPS-Apt	27.01 ± 1.27	30.57 ± 3.00	8.51
Apt	28.54 ± 2.82	30.10 ± 3.64	5.17
Control	33.47 ± 2.49	34.60 ± 1.61	3.28

Table 1B
Body visceral Index of mice after treatment with formulations.

Treatments	Weight (%) ± SD			
	Heart	Liver	Kidney	Lungs
MP	0.49 ± 0.04	4.94 ± 0.27	0.72 ± 0.06	0.78 ± 0.04
MP-Apt	0.61 ± 0.02	6.41 ± 0.57	0.80 ± 0.01	0.79 ± 0.05
MPS	0.49 ± 0.04	6.21 ± 0.33	0.71 ± 0.05	0.80 ± 0.06
MPS-Apt	0.63 ± 0.02	7.09 ± 0.03	0.77 ± 0.01	0.97 ± 0.02
Apt	0.64 ± 0.05	5.87 ± 0.46	0.73 ± 0.03	0.70 ± 0.03
Control	0.55 ± 0.023	4.38 ± 0.15	0.74 ± 0.03	0.74 ± 0.03

cells was visualized using CLSM and showing particle localization inside the nuclear region (co-localization coefficient > 0.7). The in vivo assessment of the blood profiles along with serum biochemistry demonstrated the safety of the formulations. Heart and liver-specific toxicities were however evident in the presence of SFB and Apt. The combination of SFB and Apt together with a submicron-ranged delivery system could prove to be a powerful tool in anticancer therapies. The presence of a targeted aptamer will solve the problem of non-specific effects of SFB by specifically delivering the drug to resistant tumors.

Acknowledgement

Authors would like to extend thanks to DAAD Germany, HEC

Table 1C
Complete blood count of mice after treatment with formulations.

Treatments	Hemoglobin (g/dl)	TLC (*10^9/l)	RBC (*10^{12}/l)	HCT (PCV) (%)	MCV(fl)	MCH (pg)	MCHC (%)	Platelets (*10^9/l)
MP	12.20 ± 0.10	9.60 ± 0.50	6.99 ± 0.03	43.60 ± 0.53	54.27 ± 0.38	15.27 ± 0.06	28.33 ± 0.58	652.00 ± 2.08
MP-Apt	11.27 ± 0.15	7.27 ± 0.12	5.55 ± 0.04	42.00 ± 0.10	62.23 ± 0.12	17.50 ± 0.10	28.23 ± 0.06	1015.33 ± 5.51
MPS	11.27 ± 0.21	7.20 ± 0.10	5.60 ± 0.03	39.91 ± 0.10	49.60 ± 0.10	14.67 ± 0.06	29.73 ± 0.06	910.67 ± 0.58
MPS-Apt	11.90 ± 0.10	5.70 ± 0.10	5.98 ± 0.03	42.50 ± 0.20	63.60 ± 4.59	16.80 ± 0.26	28.33 ± 0.21	1167.00 ± 5.69
Apt	12.33 ± 0.21	6.53 ± 0.06	6.99 ± 0.01	43.13 ± 0.32	62.27 ± 0.15	17.93 ± 0.06	28.80 ± 0.10	959.00 ± 9.85
Control	12.83 ± 0.31	9.67 ± 0.85	6.07 ± 0.29	44.23 ± 0.61	49.93 ± 1.17	13.90 ± 0.53	26.07 ± 0.85	1274.00 ± 20.66

Total leukocyte count (TLC).
Red blood cells (RBC).
Hematocrit (HCT).
Mean corpuscular volume (MCV).
Mean corpuscular hemoglobin (MCH).
Mean corpuscular hemoglobin (MCHC).

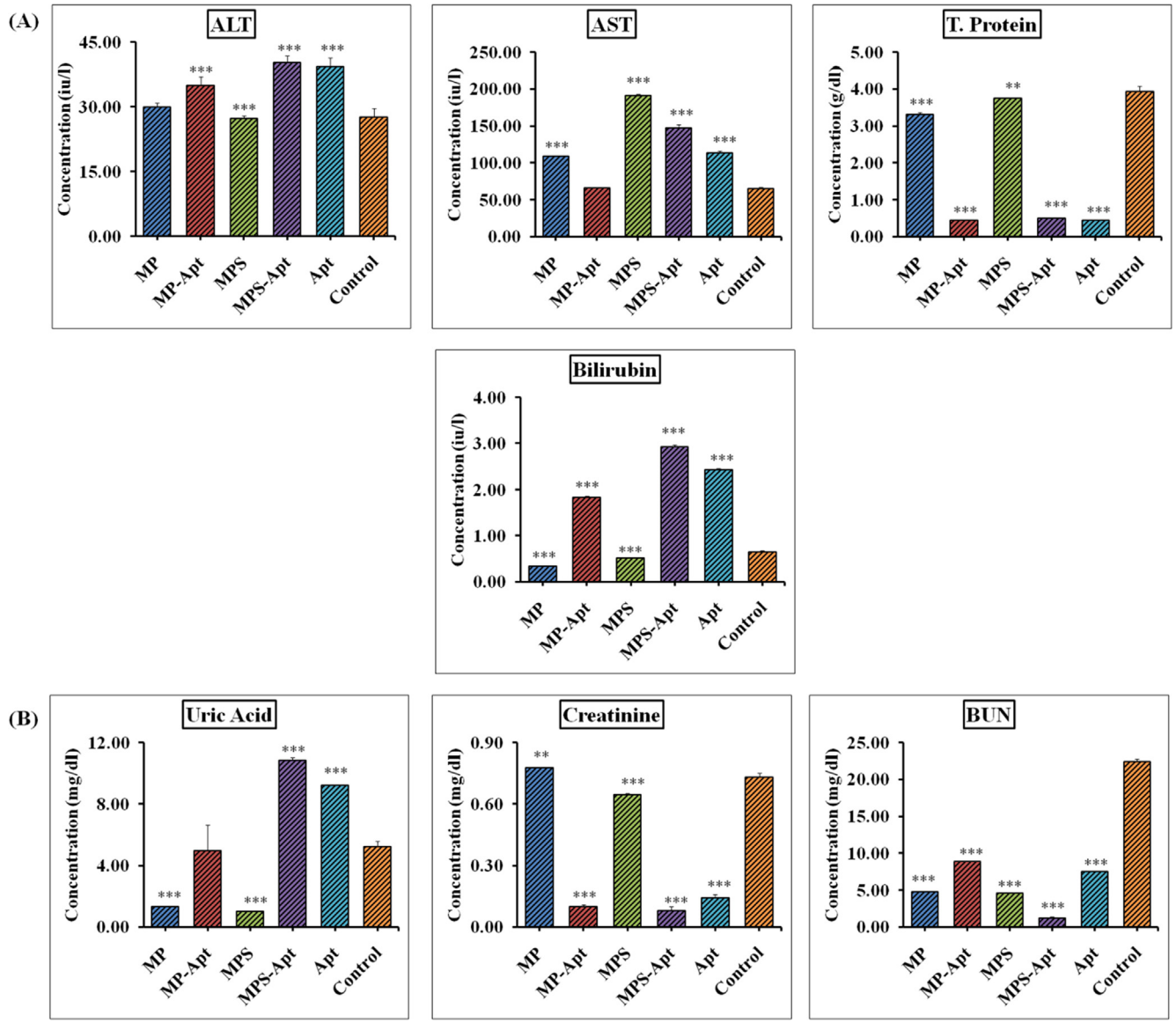

Fig. 7. Effect of microparticles (MP), surface-modified microparticles (MP-Apt), sorafenib-loaded microparticles (MPS) and sorafenib-loaded surface-modified microparticle (MPS-Apt) on blood biochemistry. Statistical differences are denoted as "**" $p < 0.01$ and "***" $p < 0.001$and were calculated using controls in each case.

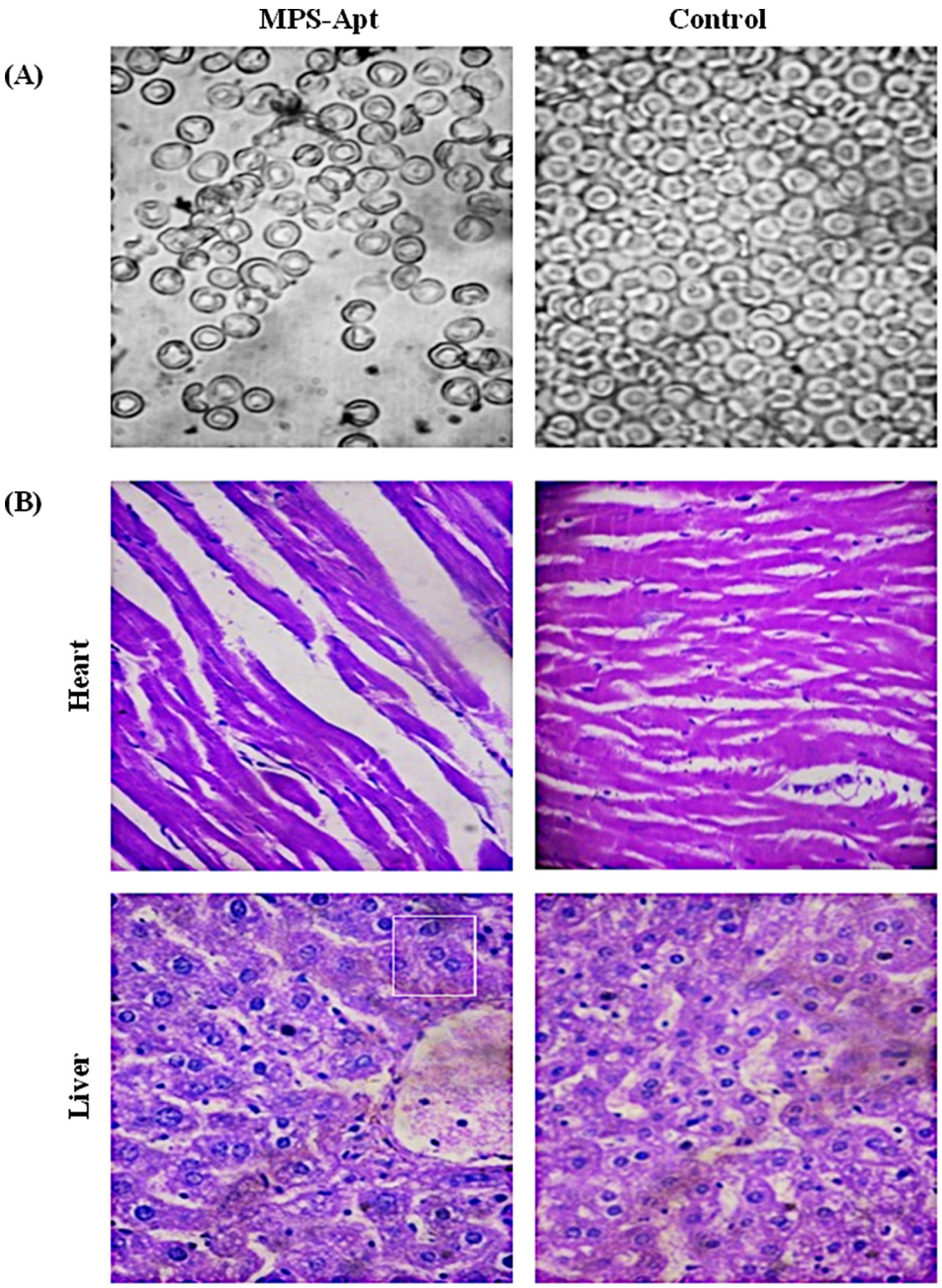

Fig. 8. Effect of different formulations on morphology and histology of cells: (A) RBC aggregation. (B) H & E staining of sorafenib-loaded surface-modified microparticle (MPS-Apt). White box indicates anisokaryosis.

Pakistan, GC University Faisalabad and overseas scholarship committee University of the Punjab for providing the support and scholarship. For technical assistance in cell culture planning and experiments, we would like to thank Mrs. Eva M. Mohr.

Declaration of Competing Interest

The authors declare no conflicts of interest.

Appendix A. Supplementary material

Supplementary data to this article can be found online at https://doi.org/10.1016/j.ejpb.2019.10.003.

References

[1] K.X. Tan, M.K. Danquah, A. Sidhu, S.Y. Lau, C.M. Ongkudon, Biophysical characterization of layer-by-layer synthesis of aptamer-drug microparticles for enhanced cell targeting, Biotechnol. Prog. 34 (2018) 249–261.
[2] C. Yu, Y. Hu, J. Duan, W. Yuan, C. Wang, H. Xu, X.-D. Yang, Novel aptamer-nanoparticle bioconjugates enhances delivery of anticancer drug to MUC1-positive cancer cells in vitro, PLoS ONE 6 (2011) e24077.
[3] V.A. Kickhoefer, M. Han, S. Raval-Fernandes, M.J. Poderycki, R.J. Moniz, D. Vaccari, M. Silvestry, P.L. Stewart, K.A. Kelly, L.H. Rome, Targeting vault nanoparticles to specific cell surface receptors, ACS Nano 3 (2008) 27–36.
[4] S.W. Song, H.J. Bae, S. Kim, D.Y. Oh, O. Kim, Y. Jeong, S. Kwon, Uniform drug loading into prefabricated microparticles by freeze-drying, Part. Part. Syst. Char. 34 (2017) 1600427.
[5] W. Bao, J. Zhou, J. Luo, D. Wu, PLGA microspheres with high drug loading and high encapsulation efficiency prepared by a novel solvent evaporation technique, J. Microencapsul. 23 (2006) 471–479.
[6] M.C. Estévez, Y.-F. Huang, H. Kang, M.B. O'Donoghue, S. Bamrungsap, J. Yan, X. Chen, W. Tan, Nanoparticle–aptamer conjugates for cancer cell targeting and detection, Cancer Nanotechnology, Springer, 2010, pp. 235–248.

[7] M.B. áO'Donoghue, A liposome-based nanostructure for aptamer directed delivery, Chem. Commun. 46 (2010) 249–251.
[8] A. Lakhin, V. Tarantul, L. Gening, Aptamers: problems, solutions and prospects, Acta Naturae (англоязычная версия) 5 (2013).
[9] M. McKeague, M.C. DeRosa, Challenges and opportunities for small molecule aptamer development, J. Nucleic Acids 2012 (2012).
[10] H. Jo, C. Ban, Aptamer–nanoparticle complexes as powerful diagnostic and therapeutic tools, Exp. Mol. Med. 48 (2016) e230.
[11] K. Mujoo, B.-K. Choi, Z. Huang, N. Zhang, Z. An, Regulation of ERBB3/HER3 signaling in cancer, Oncotarget 5 (2014) 10222.
[12] S. Acharya, F. Dilnawaz, S.K. Sahoo, Targeted epidermal growth factor receptor nanoparticle bioconjugates for breast cancer therapy, Biomaterials 30 (2009) 5737–5750.
[13] Z. Zhou, M. Jafari, V. Sriram, J. Kim, J.-Y. Lee, S.J. Ruiz-Torres, S.E. Waltz, Delayed sequential co-delivery of gefitinib and doxorubicin for targeted combination chemotherapy, Mol. Pharm. 14 (2017) 4551–4559.
[14] R. Mishra, H. Patel, S. Alanazi, L. Yuan, J.T. Garrett, HER3 signaling and targeted therapy in cancer, Oncol. Rev. 12 (2018).
[15] L. Liu, Y. Cao, C. Chen, X. Zhang, A. McNabola, D. Wilkie, S. Wilhelm, M. Lynch, C. Carter, Sorafenib blocks the RAF/MEK/ERK pathway, inhibits tumor angiogenesis, and induces tumor cell apoptosis in hepatocellular carcinoma model PLC/PRF/5, Cancer Res. 66 (2006) 11851–11858.
[16] H. Wang, S. Sun, Y. Zhang, J. Wang, S. Zhang, X. Yao, L. Chen, Z. Gao, B. Xie, Improved drug targeting to liver tumor by sorafenib-loaded folate-decorated bovine serum albumin nanoparticles, Drug Deliv. 26 (2019) 89–97.
[17] Y. Pignochino, G. Grignani, G. Cavalloni, M. Motta, M. Tapparo, S. Bruno, A. Bottos, L. Gammaitoni, G. Migliardi, G. Camussi, Sorafenib blocks tumour growth, angiogenesis and metastatic potential in preclinical models of osteosarcoma through a mechanism potentially involving the inhibition of ERK1/2, MCL-1 and ezrin pathways, Mol. Cancer 8 (2009) 118.
[18] Y.-J. Zhu, B. Zheng, H.-Y. Wang, L. Chen, New knowledge of the mechanisms of sorafenib resistance in liver cancer, Acta Pharmacol. Sin. 38 (2017) 614.
[19] M. Cervello, D. Bachvarov, N. Lampiasi, A. Cusimano, A. Azzolina, J.A. McCubrey, G. Montalto, Molecular mechanisms of sorafenib action in liver cancer cells, Cell Cycle 11 (2012) 2843–2855.
[20] S.M. Leto, L. Trusolino, Primary and acquired resistance to EGFR-targeted therapies in colorectal cancer: impact on future treatment strategies, J. Mol. Med. 92 (2014) 709–722.
[21] S.R. Pinnapireddy, L. Duse, B. Strehlow, J. Schäfer, U. Bakowsky, Composite liposome-PEI/nucleic acid lipopolyplexes for safe and efficient gene delivery and gene knockdown, Colloids Surf., B 158 (2017) 93–101.
[22] L. Duse, S.R. Pinnapireddy, B. Strehlow, J. Jedelská, U. Bakowsky, Low level LED photodynamic therapy using curcumin loaded tetraether liposomes, Eur. J. Pharm. Biopharm. 126 (2018) 233–241.
[23] S.R. Pinnapireddy, L. Duse, D. Akbari, U. Bakowsky, Photo-Enhanced Delivery of Genetic Material Using Curcumin Loaded Composite Nanocarriers, Clin. Oncol. 2 (2017).
[24] M. Mohwald, S.R. Pinnapireddy, B. Wonnenberg, M. Pourasghar, M. Jurisic, A. Jung, C. Fink-Straube, T. Tschernig, U. Bakowsky, M. Schneider, Aspherical, nanostructured microparticles for targeted gene delivery to alveolar macrophages, Adv. Healthcare Mater. (2017).
[25] G.K. Jain, S.A. Pathan, S. Akhter, N. Ahmad, N. Jain, S. Talegaonkar, R.K. Khar, F.J. Ahmad, Mechanistic study of hydrolytic erosion and drug release behaviour of PLGA nanoparticles: Influence of chitosan, Polym. Degrad. Stab. 95 (2010) 2360–2366.
[26] X. Zhu, R.D. Braatz, A mechanistic model for drug release in PLGA biodegradable stent coatings coupled with polymer degradation and erosion, J. Biomed. Mater. Res. Part A 103 (2015) 2269–2279.
[27] F.Y. Han, K.J. Thurecht, A.K. Whittaker, M.T. Smith, Bioerodable PLGA-based microparticles for producing sustained-release drug formulations and strategies for improving drug loading, Front. Pharmacol. 7 (2016) 185.
[28] T. Duan, Z. Xu, F. Sun, Y. Wang, J. Zhang, C. Luo, M. Wang, HPA aptamer functionalized paclitaxel-loaded PLGA nanoparticles for enhanced anticancer therapy through targeted effects and microenvironment modulation, Biomed. Pharmacother. 117 (2019) 109121.
[29] X. Luo, Y. Yang, F. Kong, L. Zhang, K. Wei, CD30 aptamer-functionalized PEG-PLGA nanoparticles for the superior delivery of doxorubicin to anaplastic large cell lymphoma cells, Int. J. Pharm. 564 (2019) 340–349.
[30] K. Saravanakumar, X. Hu, S. Shanmugam, R. Chelliah, P. Sekar, D.-H. Oh, S. Vijayakumar, K. Kathiresan, M.-H. Wang, Enhanced cancer therapy with pH-dependent and aptamer functionalized doxorubicin loaded polymeric (poly D, L-lactic-co-glycolic acid) nanoparticles, Arch. Biochem. Biophys. (2019).
[31] T. Wu, X. Duan, C. Hu, C. Wu, X. Chen, J. Huang, J. Liu, S. Cui, Synthesis and characterization of gold nanoparticles from Abies spectabilis extract and its anticancer activity on bladder cancer T24 cells, Artif. Cells Nanomed. Biotechnol. 47 (2019) 512–523.
[32] K.S. Mani, W. Kaminsky, S.P. Rajendran, A facile atom economic one pot multicomponent synthesis of bioactive spiro-indenoquinoxaline pyrrolizines as potent antioxidants and anti-cancer agents, New J. Chem. 42 (2018) 301–310.
[33] H.S. Shah, S.A. Joshi, A. Haider, U. Kortz, J. Iqbal, Synthesis of chitosan-coated polyoxometalate nanoparticles against cancer and its metastasis, RSC Adv. 5 (2015) 93234–93242.
[34] R. Coriat, C. Nicco, C. Chereau, O. Mir, J. Alexandre, S. Ropert, B. Weill, S. Chaussade, F. Goldwasser, F. Batteux, Sorafenib-induced hepatocellular carcinoma cell death depends on reactive oxygen species production in vitro and in vivo, Mol. Cancer Ther. 11 (2012) 2284–2293.
[35] L.I. Gordon, M.A. Burke, A.T. Singh, S. Prachand, E.D. Lieberman, L. Sun, T.J. Naik, S.V.N. Prasad, H. Ardehali, Blockade of the erbB2 receptor induces cardiomyocyte death through mitochondrial and reactive oxygen species-dependent pathways, J. Biol. Chem. 284 (2009) 2080–2087.
[36] Y. Wang, H. Yamaguchi, J.-M. Hsu, M.-C. Hung, Nuclear trafficking of the epidermal growth factor receptor family membrane proteins, Oncogene 29 (2010) 3997.
[37] B. Linggi, G. Carpenter, ErbB receptors: new insights on mechanisms and biology, Trends Cell Biol. 16 (2006) 649–656.
[38] P. Hawkins, L. Stephens, PI3K signalling in inflammation, Biochimica et Biophysica Acta (BBA)-Molecular and Cell Biology of Lipids 1851 (2015) 882-897.
[39] T. Osada, M.A. Morse, A. Hobeika, M.A. Diniz, W.R. Gwin, Z. Hartman, J. Wei, H. Guo, X.-Y. Yang, C.-X. Liu, Vaccination targeting human HER3 alters the phenotype of infiltrating T cells and responses to immune checkpoint inhibition, Oncoimmunology 6 (2017) e1315495.
[40] O.S. Adeyemi, I. Adewumi, Biochemical evaluation of silver nanoparticles in wistar rats, Int. Schol. Res. Notices 2014 (2014) 8.
[41] H.B. Shi, M. Kong, G. Chen, J. Zhao, H.L. Shi, Y. Chen, F.G. Rowan, Compound pollen protein nutrient increases serum albumin in cirrhotic rats, Gastroenterol. Res. 3 (2010) 253.
[42] E.P. Babu, A. Subastri, A. Suyavaran, K. Premkumar, V. Sujatha, B. Aristatile, G.M. Alshammari, V. Dharuman, C. Thirunavukkarasu, Size dependent uptake and hemolytic effect of zinc oxide nanoparticles on erythrocytes and biomedical potential of ZnO-ferulic acid conjugates, Sci. Rep. 7 (2017) 4203.
[43] A.V. Cardoso, M.H. Pereira, G.d.A. Marcondes, A.R. Ferreira, P.R.D. Araújo, Microplate reader analysis of triatomine saliva effect on erythrocyte aggregation, Mater. Res. 10 (2007) 31–36.
[44] K. Inomata, K. Tajima, H. Yagi, H. Higashi, H. Shimoda, K. Matsubara, T. Hibi, Y. Abe, H. Tsujikawa, M. Kitago, A pre-clinical large animal model of sustained liver injury and regeneration stimulus, Sci. Rep. 8 (2018) 14987.